



AALBORG UNIVERSITY
DENMARK

Aalborg Universitet

Mitigation measures of the electric field in the medium-voltage power module

Effect of voltage types and recommendations for designers

Huang, Zhizhao; Chen, Cai; Kang, Yong; Munk-Nielsen, Stig; Uhrenfeldt, Christian

Published in:
High Voltage

DOI (link to publication from Publisher):
[10.1049/hve2.12104](https://doi.org/10.1049/hve2.12104)

Creative Commons License
CC BY-NC-ND 4.0

Publication date:
2021

Document Version
Publisher's PDF, also known as Version of record

[Link to publication from Aalborg University](#)

Citation for published version (APA):

Huang, Z., Chen, C., Kang, Y., Munk-Nielsen, S., & Uhrenfeldt, C. (2021). Mitigation measures of the electric field in the medium-voltage power module: Effect of voltage types and recommendations for designers. *High Voltage*, 6(5), 836-849. <https://doi.org/10.1049/hve2.12104>

General rights

Copyright and moral rights for the publications made accessible in the public portal are retained by the authors and/or other copyright owners and it is a condition of accessing publications that users recognise and abide by the legal requirements associated with these rights.


- Users may download and print one copy of any publication from the public portal for the purpose of private study or research.
- You may not further distribute the material or use it for any profit-making activity or commercial gain
- You may freely distribute the URL identifying the publication in the public portal -

Take down policy

If you believe that this document breaches copyright please contact us at vbn@aub.aau.dk providing details, and we will remove access to the work immediately and investigate your claim.

ORIGINAL RESEARCH PAPER

Mitigation measures of the electric field in the medium-voltage power module: Effect of voltage types and recommendations for designers

Zhizhao Huang¹  | Cai Chen¹ | Yong Kang¹ | Stig Munk-Nielsen² | Christian Uhrenfeldt²

¹State Key Laboratory of Advanced Electromagnetic Engineering and Technology, Huazhong University of Science and Technology, Wuhan, China

²Department of Energy Technology, Aalborg University, Aalborg, Denmark

Correspondence

Cai Chen, State Key Laboratory of Advanced Electromagnetic Engineering and Technology, Huazhong University of Science and Technology, Luoyu Road 1037, Wuhan, China.
Email: caichen@hust.edu.cn

Associate Editor: Jianying Li

Funding information

National Natural Science Foundation of China, Grant/Award Number: 52077094

Abstract

In the medium-voltage silicon carbide device power module, the higher voltage level will induce higher electric field stress in critical internal points such as the edge of the conductor on the direct bonded copper (DBC) substrate. This can lead to partial discharge and subsequently accelerated ageing of the insulating medium in the module. Therefore, it is important to reduce the high electric field strength. Herein, the related technical methods of electric field control are reviewed and compared by combining the ease of implementation in real power module and the field control effect. In addition, systematic explanations of the electric field drift and influencing factors of the electric field strength under different voltage types within different module structures are presented. Finally, for half-bridge power modules with different substrates structures, suggestions on how to implement non-linear field-dependent materials to reduce the electric field strength are given.

1 | INTRODUCTION

The 4H-SiC material for power devices has an order of magnitude, higher critical electrical breakdown field (2×10^6 to 4×10^6 V/cm) and higher switching frequency than conventional silicon materials [1]. These characteristics make SiC devices gain more attention for medium-voltage (MV) applications, such as high speed MV motor drives, MV dc micro-grids and traction solid-state transformers [2–5]. Some customised MV power modules and MV converters have been designed based on 10–15 kV SiC MOSFETs or SiC IGBT [6–8]. One of the challenges of applying high voltage SiC devices is the higher risk of unacceptable partial discharge (PD) activities within the module compared with Si-IGBT devices, especially when the devices are packaged in the compact size with higher voltage. High activity of PD degrades the insulation materials [9–11]. Besides, repetitive PD will lead to the failure of the cover and substrate materials, such as cracking of the ceramic substrate [12]. Thus, it is

important to reduce the activity of PD in power module design and new insulation solutions are required.

In the power module, there are two kinds of insulation materials: ceramic substrate and silicone gel as presented in Figure 1. Direct bonded copper (DBC) substrate is used to realise the electric connection and the isolation from the circuit pattern to the baseplate. The ceramic material in the DBC substrate is usually aluminium nitride (AlN) or alumina (Al₂O₃). Silicone gel is used to encapsulate the inside of the module to prevent electrical discharges in air and to protect semiconductors, DBC substrate, and connections against humidity, dirt, and vibration.

G. Mitic and G. Lefranc have proved that the highest electric field strength in a power module is typically localised at the metallisation edge of the ceramic substrates [13, 14]. This is also called triple point where the ceramic, the copper and the encapsulation material meet [15]. Higher electric field strength means higher probability of PD. Besides, when the electric field exceeds the limitation of insulation media, breakdown of

This is an open access article under the terms of the Creative Commons Attribution-NonCommercial-NoDerivs License, which permits use and distribution in any medium, provided the original work is properly cited, the use is non-commercial and no modifications or adaptations are made.

© 2021 The Authors. *High Voltage* published by John Wiley & Sons Ltd on behalf of The Institution of Engineering and Technology and China Electric Power Research Institute.

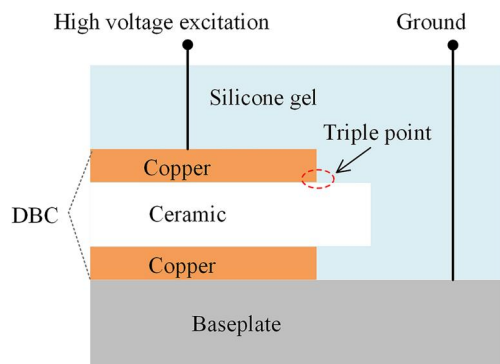


FIGURE 1 Illustration of the triple region at the direct bonded copper substrate

dielectric material might happen in the form of complete breakdown or partial discharges, which will degrade the material permanently. Thus, many researchers focussed on how to control the high electric field at the triple point.

Usually, increasing the insulation distance can reduce electric field stress. However, the relationship between the maximum electric field strength and the thickness of the ceramic is not a linear correlation [16]. This method will lead to higher thermal resistance of the chips. Besides, the maximum thickness of the ceramic substrate has been limited in practice due to the process' feasibility. Stacking DBC substrates can expand the total thickness of the ceramic substrate. Thus, it can be used to reduce the electric field strength at the triple point [17–20]. PD tests revealed that the partial discharge inception voltage (PDIV) of the stacked DBC substrates is nearly two times higher than that of a single Al_2O_3 with the same total ceramic thickness [17]. This method has been implemented in a high-density 10 kV SiC MOSFET power module, which realised good thermal performance by using advanced cooling design [19]. Moreover, Amol Deshpande et al. proposed stacked DBC cavitied substrates, which allow bypassing the need for a voltage-clamped interlayer metallisation. However, they did not address the challenges in avoiding PD sensitive air pockets in these cavities during the encapsulation of real power module architectures [20]. By using the field plate at the edge metallisation of DBC substrates, the PDIV can be increased by about 15% [18]. However, field plate structure requires a lot of space, as shown in reference [18], which reported that for a ceramic thickness of 1 mm, the length of the field plate with the maximal effect is about 4 mm. This contradicts the compact volume design of the power module. Some other novel modifications of ceramic substrates have also been proposed to control the electric field, such as protruding substrate [19], mesa structure at the ceramic [22, 23], and 3D module layout [24]. However, these structures require complicated processing techniques, which is not feasible in the current fabrication process.

Except for the geometric methods above, applying functional materials in the high-stress region is also an effective way to control the electric field. Functional materials include linear functional materials and non-linear functional materials. G.

Mitic proposed that using the linear resistive functional layer (amorphous silicon coating) deposited on the top of the DBC substrate could help reduce the electric field stress [14]. In order to homogenise the electric field strength, the electric conductivity of the resistive layer should be carefully selected. Very high conductivity will lead to non-negligible leakage current, and very low conductivity will have no effect of modifying the electric field. Besides, linear resistive field control depends on the frequency and its advantage reduces with increasing frequency [25]. For these reasons, non-linear field-dependent conductivity (FDC) materials have been developed to control the electric field. In Ref. [26–28], Thomas Christen et al. systematically describe the characteristics, theories, simulations and applications of non-linear FDC materials. Mona Ghassemi et al. also present a number of simulation-based studies on non-linear FDC fillers application in power module packaging [29–32]. In paper [29], they indicated that FDC filler is more effective under DC voltage rather than under AC condition but did not elaborate on the reasons and how to apply FDC filler to the real power module. Capacitance field control is another way of electric field control. In Ref. [33], U. Waltrich et al. use high dielectric constant epoxide resin (relative permittivity 4.4) as the linear permittivity functional material to cover the DBC trench. This epoxide resin coating layer works as a refractive field control and reduces the field strengths in the most critical section around the triple point. Phase-resolved partial discharge (PRPD) measurement results showed that this could lead to improvements in PDIV of at least 20% [33]. The high permittivity coating layer relieves high electric field stress adjacent to the copper metallisation, However, it leads to higher electric field stress in the gel and in particular the weak interface between the layer and the gel encapsulation [34]. This means a high permittivity material as a coating layer may not be efficient [34]. Wang et al. used barium titanate as a field-dependent permittivity (FDP) material to fill the silicone gel. They reported that the silicone gel containing 15% by volume of barium titanate can achieve 60% improvement in PDIV [35]. However, FDP fillers are only useful for AC voltage stress [35].

In the real power module, the operation voltages contain both AC and DC voltages. Besides, the power module based on stacked DBC structure brings the new voltage stress type between the power terminal and the baseplate. Although the functional materials have great potential to control the electric field strength, it is still not clear how to use it in the power module with different voltage stresses. Thus, we will systematically analyse the effect of the linear and the non-linear field-dependent functional materials on the different voltage types at room temperature and give recommendations for applying functional materials to power modules with different structures.

This paper is organised as follows: Section 2 will review the state of electric field management and evaluate the feasibility of practical applications in power module. Different voltage stress types in real module with different configurations also have been clearly identified. In Section 3, a brief

explanation on electric field evolution will be given to explain how conductivity and permittivity of covering materials influence the electric field under different voltage types. In Section 4, the effect of field-dependent materials on electric field management will be evaluated by simulations, and recommendations for implementation of field-dependent materials in power modules with different substrate configuration will be presented. Finally, the conclusion will be presented in Section 5.

2 | STATE OF ELECTRIC FIELD MANAGEMENT AND THE VOLTAGE STRESS TYPES IN THE REAL POWER MODULE

2.1 | State of the electric field management

Several ways have been proposed so far to reduce the maximum electric field strength at the triple point in the power module, which can be divided into three categories: (1) stack DBC substrates, (2) modify the DBC geometric parameters, and (3) modify the characteristics of the insulation material around the triple point.

According to the processing difficulty in the real module and the effect on controlling the electric field, the comparison results of different methods are given in Table 1. Stacked DBC substrates can be joined by soldering, sintering or by direct bonding [17], which is not complicated to realise. However, thermal resistance will increase with the increase of total

thickness of ceramic; it needs to be optimised by good thermal management [19]. Some other methods of modifying geometric parameters of DBC substrates are also easy to implement in real modules, but with little effects on the electric field strength because for a given ceramic thickness the voltage stress across the ceramic is a key contribution to the electrical field at the triple point. Some novel DBC substrates could significantly reduce the maximum electric field, such as the protruding substrate [21] and the mesa substrate [22, 23], but these technologies are currently difficult to implement in real power modules. Field grading substrate was first proposed by Z. Valdez-Nava directly integrated a new region with different dielectric properties into the basic ceramic substrate [23]. However, at present, this technology has not yet been achieved, and there are no achievable samples.

Non-linear FDC and FDP fillers can be mixed within silicone gel or epoxy resin, as long as a suitable method is used to ensure dispersion into solution and prevent aggregation and sedimentation. Moreover, these fillers also have a good effect on electric field control. So, the effect of linear fillers as well as non-linear FDC and FDP fillers on electric field control is focused on here, and the attempts to connect these fillers with actual modules with different electrode configurations.

2.2 | The voltage stress types in real power module

All the above-mentioned field management methods are aimed at reducing the maximum electric field at the triple point.

TABLE 1 Comparison of different electric field control methods

Category	Methods	Easy of Processing	Effect on E_{\max}
Stacked DBC	Stacked DBC [17–20]	☆☆☆	☆☆☆☆
Geometric parameters	Thickness of conductor [16]	☆☆☆☆	☆
	Thickness of ceramic [16]	☆☆☆☆	☆☆
	Shape of the edge [16]	☆	☆☆
	Fillet the metal corner [12, 37]	☆☆☆☆	☆
	Conductor layer offset [12, 16]	☆☆☆☆	☆☆
	Protruding substrate [21]	☆	☆☆☆
	Mesa substrate [22, 23]	☆	☆☆
	3D module layer [23]	☆	☆☆
	Field plate [18]	☆☆	☆☆
Material parameters	Higher dielectric constant coating layer [33, 36]	☆☆	☆☆
	Linear resistive layer [14]	☆☆	☆☆
	Linear permittivity layer [28, 33]	☆☆	☆☆
	Field grading substrate [23]	☆	☆☆
	Non-linear FDC fillers [26–32]	☆☆☆☆	☆☆☆☆
FDP fillers (FDP) [35]	☆☆☆☆	☆☆☆☆	

Note: More stars mean easier to process or better effect.

Abbreviations: DBC, direct bonded copper; FDC, Field-dependent conductivity; FDP, field-dependent permittivity.

However, so far little considerations have been given to the actual voltage stress types in the real power module, and it has little connection with the configuration of the terminals within the power module.

The half-bridge (HB) power module is set as a study case to show the real voltage stresses clearly. Conventional HB power module is based on a single DBC substrate. However, recently more power modules based on stacked DBC substrates have been developed [17–20], which brings new voltage potential combinations. Two basic DBC substrates and voltage stress types for different terminals in an HB power module structure are shown in Figures 2 and 3, respectively. Figure 2 represents the single DBC substrate as case A. In case A, the voltage stress type between DC + terminal metal and bottom ground baseplate is DC voltage; for Output terminal, there is always unipolar square wave voltage stress; there is no voltage stress for DC- terminal. Figure 3 is the stacked DBC substrates as case B. It should be noted that it is better to fix the middle copper layer at $0.5 \times V_{DC}$ voltage in stacked DBC substrates [19]. It

is possible to mainly eliminate the electric field stress from horizontally adjacent copper areas by securing sufficient track width. In this case, the most critical field stress is mainly caused by two adjacent conductors across the ceramic with different voltage potentials. Thus, Figure 3 only shows the voltage stresses between top coppers from different terminals and the middle copper with a fix $0.5 \times V_{DC}$ voltage potential. The voltage stresses in case B are different from case A. The voltage stress from the DC + terminal copper to the middle copper layer has been reduced to half of V_{DC} , while the voltage stress from the DC terminal to the middle layer has changed from no voltage stress to negative $0.5 \times V_{DC}$ voltage. Besides, there is bipolar square wave voltage stress for the output terminal. Here, all these voltage stresses can be divided into three types: (1) DC voltage; (2) pure AC voltage (zero average voltage), like bipolar square wave voltage as shown in Figure 3(b); (3) DC + AC voltage, like unipolar square wave voltage, as shown in Figure 2b. All these square wave voltages used in simulation comprise 50% duty cycle for simplification.

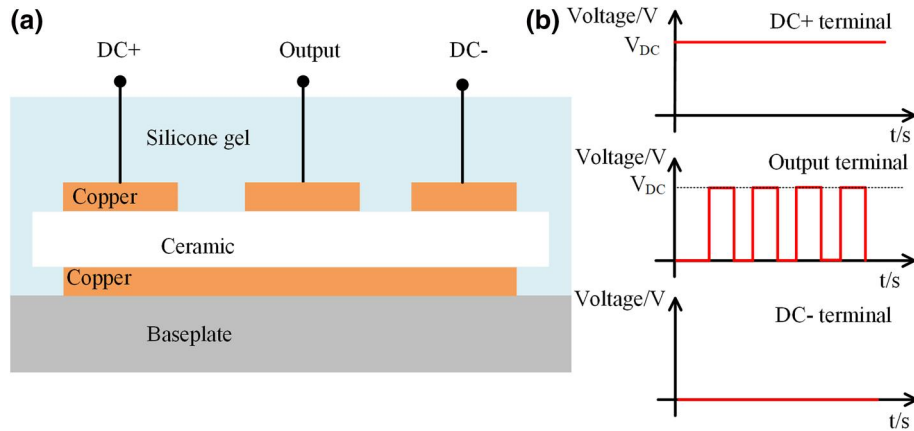


FIGURE 2 Single DBC substrate module: (a) schematic of basic substrate structure, (b) illustration of different voltage stress types

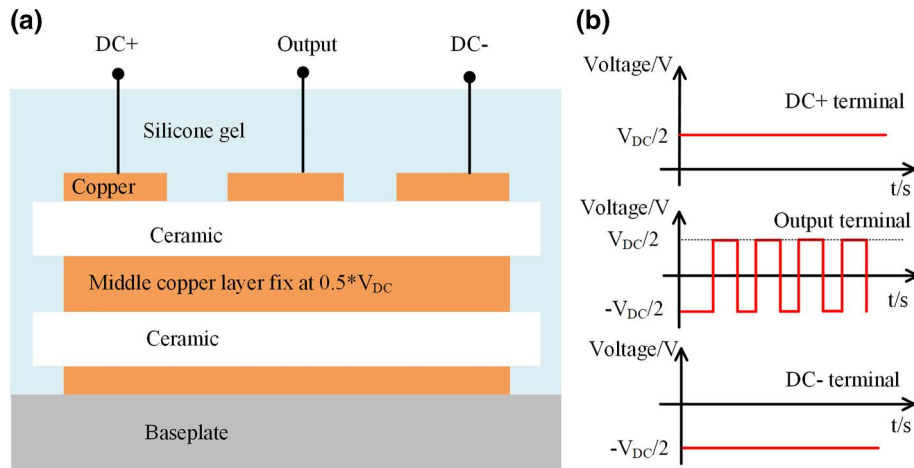


FIGURE 3 Stacked double bonded copper substrate module: (a) schematic of basic substrate structure, (b) illustration of different voltage stress types

3 | NUMERICAL CALCULATION OF ELECTRIC FIELD DISTRIBUTION AND EVOLUTION

In this section, prior knowledge about electric dynamic will be reviewed, a clear explanation about evolution of the electric field under different voltage stresses and how it is influenced by the characteristics of the encapsulation material will be shown. The discussion is supported with simulations performed in Comsol® Multiphysics. For that reason, the represented equations follow the nomenclature used in this software.

3.1 | Charge relaxation theory

We assume that the involved materials have uniform conductivity and permittivity. The fundamental equation involved is Ohm's law for the electric conduction current density \mathbf{J}_c

$$\vec{J}_c = \sigma \vec{E} \quad (1)$$

where σ is the conductivity of the involved material, and \mathbf{E} is the electric field. According to Charge Conservation Law,

$$\int_{\partial V_s} \vec{J}_c \cdot d\vec{S} = -\frac{\partial}{\partial t} \int_{V_s} \rho dV_s \quad (2)$$

where ρ is the electric charge density, V_s in Equation (2) presents the volume, and $S = \partial V_s$ is the surface of the volume V_s . Then, Equation (2) can be formulated in the following form:

$$\frac{\partial \rho}{\partial t} + \nabla \cdot \vec{J}_c = 0 \quad (3)$$

According to Gauss's law from Maxwell equations,

$$\nabla \cdot (\epsilon \vec{E}) = \rho \quad (4)$$

where ϵ is the permittivity of the involved material. By combining Equations (1), (3) and (4), the following differential equation for the space charge density in a homogeneous medium can be given:

$$\frac{\partial \rho}{\partial t} + \frac{\sigma}{\epsilon} \rho = 0 \quad (5)$$

For an initial excess charge ρ_0 , this equation has the solution

$$\rho(t) = \rho_0 e^{-t/\tau} \quad (6)$$

where

$$\tau = \frac{\epsilon}{\sigma} = \frac{\epsilon_r \epsilon_0}{\sigma} \quad (7)$$

TABLE 2 Material properties and relaxation time [16]

Material	Relative permittivity ϵ_r	Electric conductivity σ [S/m]	Time constant τ [s]
AlN ceramic	8.9	10^{-11}	7.9
Silicone gel	2.7	10^{-13}	239

where $\epsilon_0 = 8.854 \times 10^{-12}$ F/m is the vacuum dielectric constant and ϵ_r is the relative permittivity of the material. τ is the charge relaxation time, also called time constant. It characterises the relaxation time for exponential convergence of the surrounding material to screen or redistribute the excess charge.

When modelling real-world devices, there is not only the intrinsic time scale of the charge relaxation time but also an external time scale T at which a device is energised. It is the relationship between the external time scale and the charge relaxation time that determines which formula is to be used to solve the charge distribution. Table 2 shows the characteristics of AlN substrates and silicone gel commonly used in power modules at room temperature. It can be seen that the time constant is very large compared with the switching cycle in the operation of the power module, which is in the order of 10^4 larger.

In most applications of the HB power module, the switching frequency is very high, generally greater than a few kHz, even hundreds of kHz. Thus, the period time T of the pure AC voltage (like bipolar square wave voltage) is satisfied $T \ll \tau$, the space charge density has no sufficient time to adopt to the new voltage distribution before the polarity of the external potential is inverted. In this case, the electric conduction current can be neglected compared to the displacement current. The classical Poisson's equation can be derived as shown in formula (8), the space charge density is governed by the permittivity of the involved materials. Since the space charge density will change the electric field distribution, the electric field strength is determined by the permittivity of the involved materials.

$$-\nabla \cdot (\epsilon_0 \nabla V - \vec{P}) = \rho \quad (8)$$

where V is the voltage potential, and \mathbf{P} is the polarization strength.

If the external time scale is much larger than τ , as $T \gg \tau$, the stationary solution to the equation of continuity has been reached. In the stationary state, a general form Ohm's law states that

$$\vec{J} = \sigma \vec{E} \quad (9)$$

where \mathbf{J} is the electric conduction current density. The static form of the equation of continuity then reads

$$\nabla \cdot \vec{J} = -\nabla \cdot (\sigma \nabla V) = 0 \quad (10)$$

For DC voltage stress, the time scale can be seen as infinite, so there is enough time to reach the static situation. The

electric field distribution is determined by the conductivity of the material as formula (9) described. That means resistive field control could be used to change the electric field strength under DC voltage stress.

If the charge relaxation time is comparable to the external time scale or the observation time, the involved equation is

$$-\nabla \cdot \frac{\partial}{\partial t} (\epsilon_0 \nabla V + P) - \nabla \cdot (\sigma \nabla V) = 0 \quad (11)$$

In this situation, the electric field strength is determined by the permittivity as well as the conductivity of involved materials, which necessitates systematic numerical analysis. Further, as will be discussed, in heterogeneous structures like power modules geometry and material combinations add to the complexity.

3.2 | Electric transient simulation

In order to understand the effect of conductivity and permittivity on the dynamic electric field's evolution, a step voltage is used to simulate the process of the electric transient to explain which parameters influence the electric field and when it happens. Figure 4 shows the 2D simulation model structure. Four measurement points P1–P4 with a distance of 50 μm from the triple point were used to ensure a mesh-independent evaluation procedure [14]. The upper metal was energised by a step voltage which starts from 0 V and rises after 0.1 s to 10 kV during 1 μs . Afterwards, the voltage level stays at 10 kV until 1000 s.

In the simulation, the mesh size at the triple point is 50 μm , and it is assumed that the material parameters of silicone gel can be changed. Figure 5 shows the trends of electric field strength at four measurement points with time under different relative permittivity and different conductivity of the silicone gel. As shown in Figure 5, during the voltage transition time, the electric field value is mainly determined by the relative permittivity, and the electric field value decreases with the increase of the relative permittivity of silicone gel. After the voltage is stable, the electric field strength is determined by the conductivity. The higher the conductivity of silicone gel, the lower the steady state electric field strength. Besides, the time of electric field changed to the settled value is different, which is influenced by the time constant of involved materials.

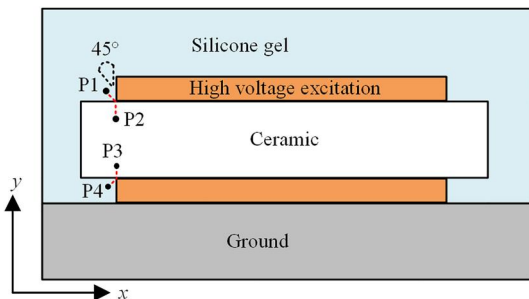


FIGURE 4 Simulation model structure

Figure 6a,b illustrates the electric field distribution at the edge of the DBC metallisation during the transient time and settled time, respectively, using the non-modified material parameters presented in Table 2. In order to view the electric field distribution at the interface between silicone gel and ceramic, the electric field lines between the edge of the high-voltage electrode (solid red line) and the edge of the ground electrode (red dashed line) were selected in the Comsol $\text{\textcircled{R}}$ Multiphysics simulation results. It can be seen that the electric field changes from refractive dominant to current sharing/expanding dominant. These figures also show how the field redistribution is governed by both geometric structures as well as the different material properties which combined, dictate a more complex transient behaviour than that predicted from the pure material relaxation time constants. In an electric circuit analogy, this is like the dynamics of a multicomponent capacitive/resistive network which may not be explained fully from single RC pair dynamics.

3.3 | Electric field under bipolar square wave voltage

Consider the stacked DBC substrates case B shown in Figure 3. There is bipolar square wave voltage stress between the output terminal and middle copper. In practical applications, the power module will continue to switch, so it is important to understand how the electric field changes over time. Figure 7a is the electric field value at measurement point P1 under 1 Hz 10 kV bipolar square wave voltage excitation. Figure 7b is the enlarged view of Figure 7a and contains the E_x and E_y . E_x represents the component of the electric field in the x direction, E_y represents the y -direction component. The directions of E_x and E_y are opposite in the positive and negative half cycles, indicating that the direction of the electric field is also opposite in the positive and negative half cycles. Under 50% duty cycle bipolar square wave voltage, the average voltage value is zero (which means pure AC voltage stress). As a consequence, it is observed that the electric field does not display any long-term drift. The reason, as commented above, is that for small time scales like switch period, the charges do not have time to redistribute to any significant degree because the switching period time is much small than the relaxation time. For large time scales comparable with relaxation time, the distribution of charges has enough time to change. However, the average value of 50% duty cycle bipolar square wave voltage excitation is zero, so the charges are still not changed, the electric field is changed only by the changing of excitation voltage and polarization induced displacement currents.

Since polarization effects dominate under pure AC stress conditions, for the stacked DBC substrates case B and electric field around the output terminal, the way to reduce the electric field is to optimise the relative permittivity of involved cover materials. Assuming that the dielectric constant of the silicone gel can be adjusted, Figure 8 shows the maximum electric field at P1–P4 with different relative permittivity of silicone gel under 50% duty cycle bipolar square wave voltage excitation. The electric field strengths at all measurement points are reduced by

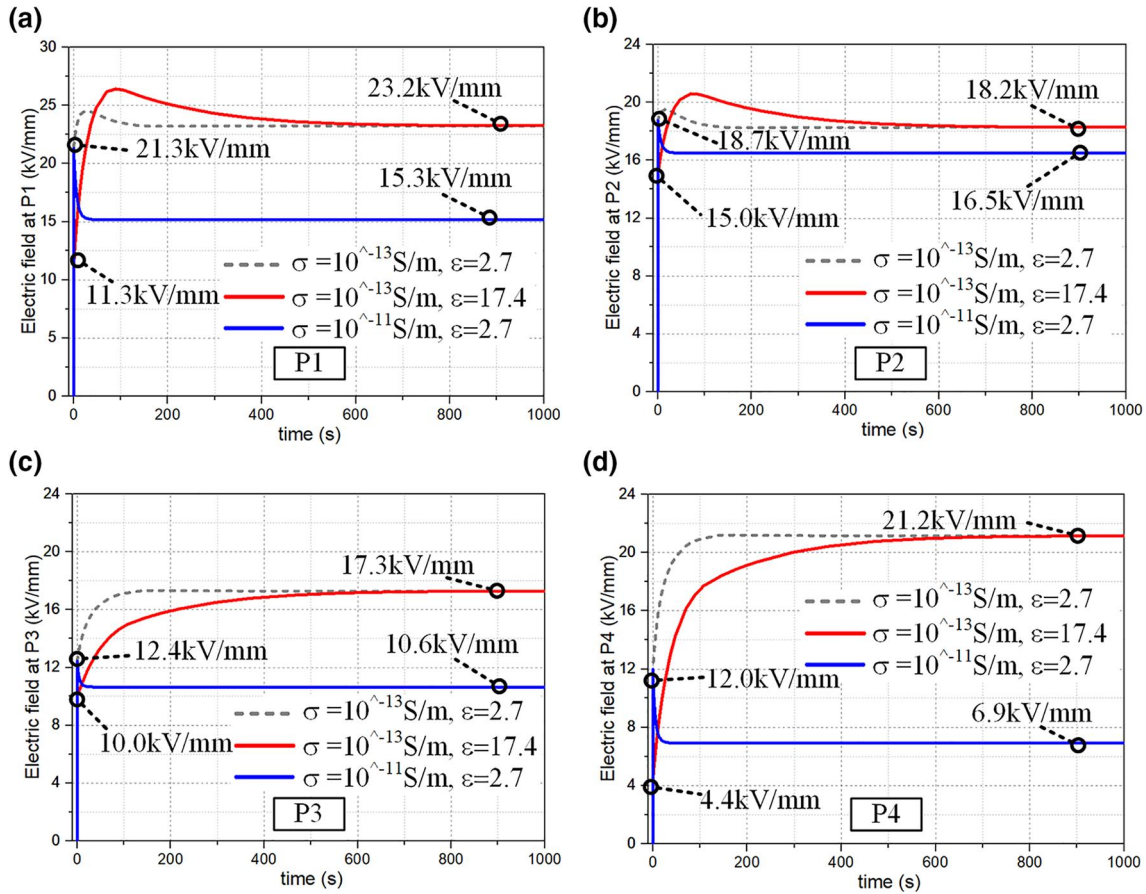


FIGURE 5 Electric fields under step voltage with different relative permittivity and conductivity of gel: (a) P1, (b) P2, (c) P3, (d) P4

increasing the relative permittivity of the silicone gel. That means for the output terminal in case B configuration, if the voltage stress is 50% duty cycle bipolar square wave voltage, increasing the relative permittivity of covering material is an effective way to reduce the maximum electric field. However, according to the author's best knowledge, there are no commercially available silicone gels or other types of encapsulation with a higher relative permittivity, most of the encapsulation materials have a low relative permittivity small than 3. However, the permittivity of the encapsulation can be increased by adding filler particles of higher permittivity. Fillers could be linear, high permittivity solid particles or could be non-linear permittivity particles. There is one way to increase the relative permittivity of silicone gel as reported in Ref. [35]; using barium titanate as non-linear permittivity particles into the base silicone gel could increase the relative permittivity and form the FDP stress-relieving dielectric material. This implies that high permittivity or non-linear FDP type fillers are suited to mitigate the electric field strength under this type of voltage stress.

3.4 | Electric field under unipolar square wave voltage

In the HB power module based on a single DBC substrate, the voltage stress between the output terminal and baseplate is the

unipolar square wave voltage. Figure 9 shows the electric field under 1 Hz 10 kV unipolar square wave voltage and the electric field under 5 kV step voltage, using the material characteristics of the non-modified material parameters presented in Table 2. Figure 10a is the electric field value difference between these two electric field values. Figure 10b is the electric field under 5 kV bipolar square wave voltage. Upon comparing Figure 10a,b, it can be seen that the absolute value of electric field strength is equal, which means that the electric field under 10kV unipolar square wave voltage can be seen as the sum of the electric field under 5 kV bipolar square wave voltage and electric field under 5 kV ($V_{DC} \times$ duty) DC voltage. Thus, the mix DC + AC voltage excitation can be divided into two parts, one is the DC voltage ($V_{DC} \times$ duty), the other is the AC voltage part.

1Hz square wave voltage is used for long-term observation of the simulation results. A square wave with a kilohertz frequency could also be used. However, it will consume a lot of computer resources and even run out of memory. For example, if a 1 kHz square wave voltage excitation is used and the simulation end time is set to 100 s, it means 100,000 cycles need to be calculated, and the massive data also need large memory to be stored. Figure 11 compared the electric field intensity under 1 kHz square wave voltage and 1 Hz square wave voltage at different simulation times. The electric field value under 1 Hz

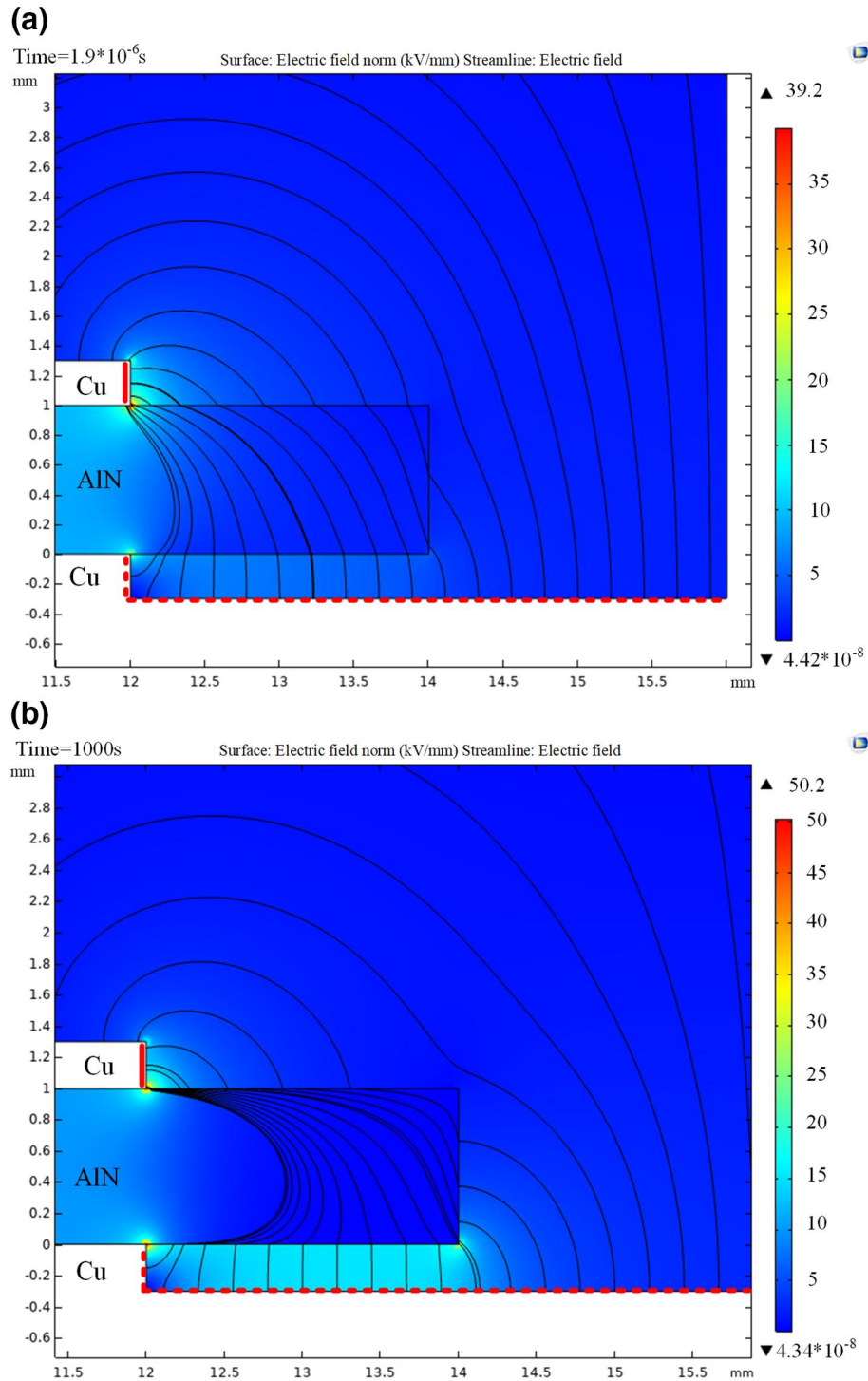


FIGURE 6 Electric field distribution (a) during the voltage transient time and (b) after the voltage has been settled

frequency is equal to that under 1 kHz (or higher frequency). The reason is that for the selected material, the time constant of the material far exceeds the period of 1 Hz and 1 kHz frequency, and for the material with a time constant between these different periods this observation will not hold. Therefore, a 1 Hz square wave voltage frequency is adopted in the simulation to avoid the limitation of computer resources and save simulation time.

Since the mixed DC + AC voltage excitation can be decoupled into a DC part and an AC part, it is interesting to see how the dielectric constant and conductivity of silicone gel influence the electric field under unipolar square voltage. Figure 12 depicts the electric fields at P1 under 1 Hz 10 kV unipolar square wave voltage and 5 kV step voltage when the gel relative permittivity is 17.4. Compared with Figure 9, the average electric field (12.65 kV/mm) is

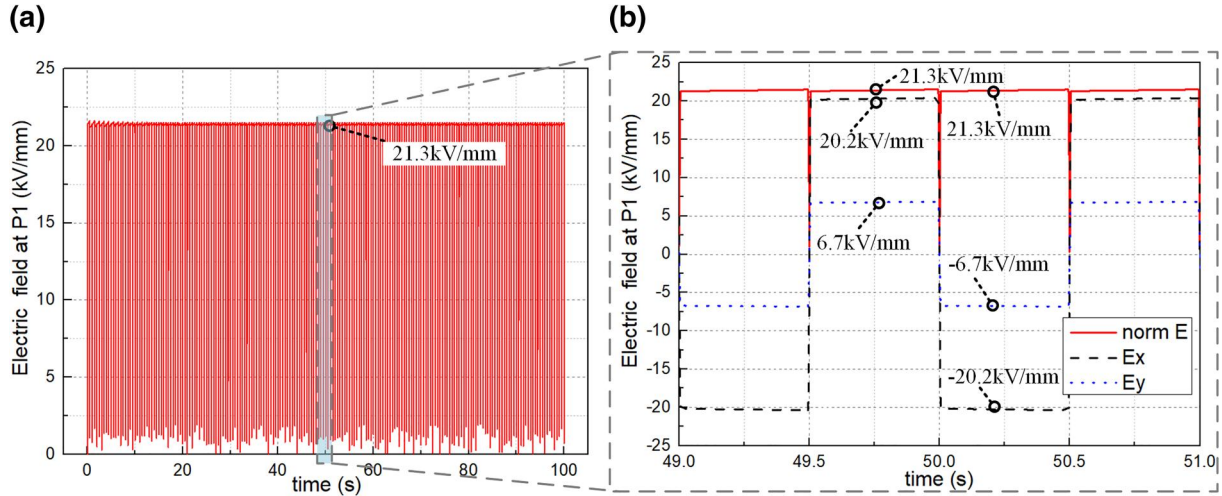


FIGURE 7 Electric field strength at P1 under bipolar square wave voltage: (a) electric field intensity, (b) illustration of the direction

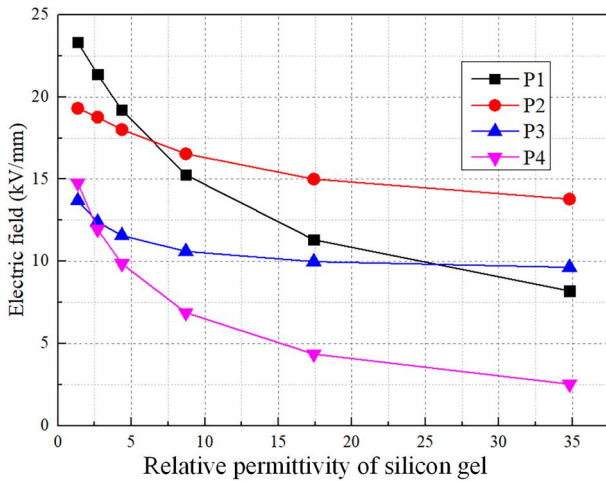


FIGURE 8 Maximum electric field value at four measurement points under bipolar square wave voltage with different relative permittivity of silicone gel

not changed and is still equal to the electric field (12.5 kV/mm) under $V_{DC} \times \text{duty}$ (5 kV). However, the peak-to-peak electric field value is decreased from (21.2 kV/mm) to 11.3 kV/mm by the increase of the relative permittivity of silicone gel, which may have a beneficial effect on the electric field stress in the material. The electric fields at P1 under 1 Hz 10 kV unipolar square wave voltage and 5 kV step voltage when the conductivity of silicone gel is changed to 10^{-11} S/m are shown in Figure 13. Because the conductivity determined the electric field value under DC voltage, the increase of conductivity of gel decreases the electric field value under $V_{DC} \times \text{duty}$ (5 kV), thus also decreasing the maximum electric field value by reducing the long-term average electric field value.

Corresponding to the output terminal in the power module with a single DBC substrate, when the converter continues to operate, the average electric field value will drift towards the electric field under an equivalent steady voltage, which is corresponding to the average voltage (the duty cycle multiplied with V_{DC} if the pulse width is constant). As the simulation results are shown from Figure 9 to Figure 13, the maximum electric field is not only determined by the average electric field value but also the peak-to-peak electric field value. Thus, both relative permittivity and conductivity of the silicone gel should be increased in order to efficiently decrease the electric field strength under unipolar square wave voltage.

4 | RECOMMENDATIONS FOR IMPLEMENTING NON-LINEAR FIELD-DEPENDENT MATERIAL IN POWER MODULES

Although many research papers have simulated the effect of non-linear FDC and FDP materials in electric field management, little considerations are given to how to implement these materials in the real module. In this section, after showing two simulation results about the influence of non-linear FDC and FDP materials on electric field control, recommendations for the implementation of non-linear electric field-dependent materials in the power module with different substrate configurations are presented.

4.1 | Simulations of FDC and FDP fillers

For the non-linear FDC material, the relation between its conductivity, $\sigma(E)$, and $E(x, y)$ within the layer is given by [28, 32].

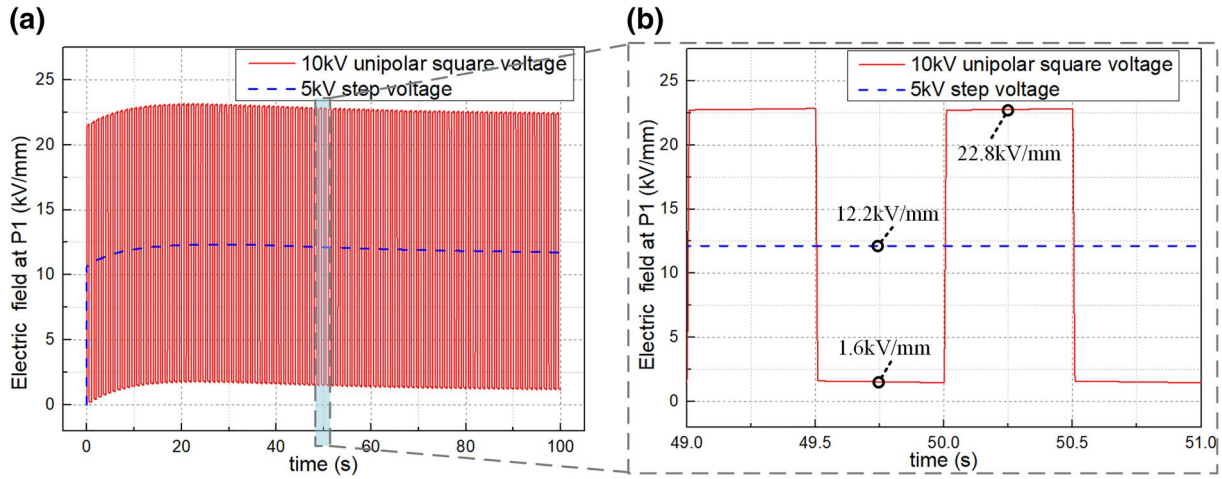


FIGURE 9 Electric fields at P1 under 1 Hz 10 kV unipolar square wave voltage and 5 kV step voltage with the non-modified material

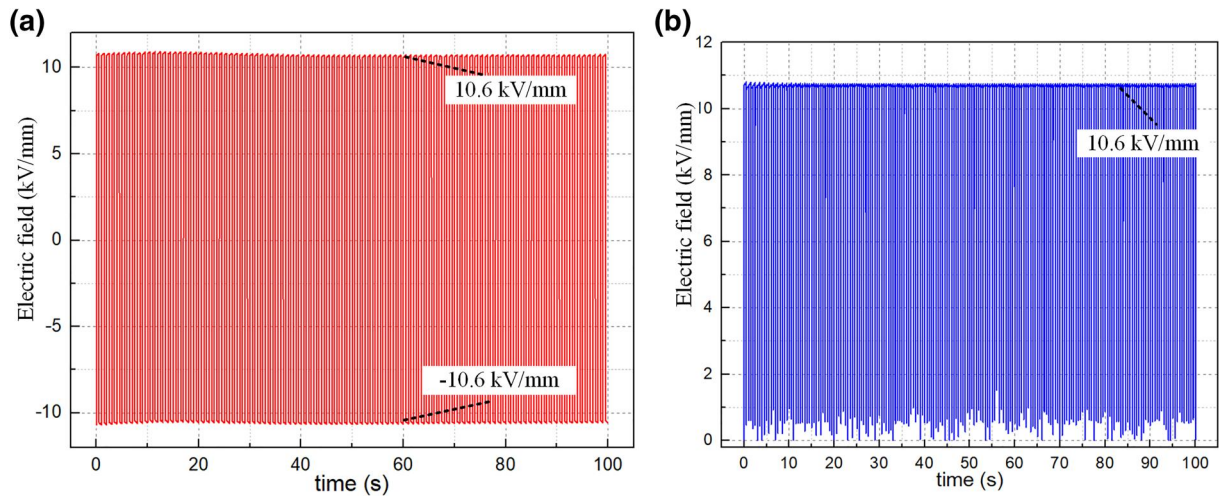


FIGURE 10 (a) Electric field value difference between electric field under 10 kV unipolar square wave voltage and electric field under 5 kV step voltage. (b) Electric field at P1 under 5 kV bipolar square wave voltage

$$\sigma(E(x, y)) = \sigma_0 * \left(1 + \left(\frac{E(x, y)}{E_b} \right)^{\alpha-1} \right) \quad (12)$$

where σ_0 is the linear conductivity. Assuming zinc oxide (ZnO) microvaristor as the fillers, $\sigma_0 = 3.3 \times 10^{-11}$ S/mm [27]. To achieve an effective electric field grading effect independent of frequency for most applications, $\alpha > 10$ should be chosen [27, 28]. Thus $\alpha = 12$ is considered for simulation. The simulation model is shown in Figure 14, the silicone gel around the edge of the DBC are filled by field-dependent material. Since the non-bridging, non-linear FDC layer will result in electric field enhancement in the bottom copper layer edge [32], the bridging non-linear FDC layer is adopted in this simulation. The switching field E_b should be equal to the ratio of the maximum applied voltage to the layer length [28]. In this simulation, for an applied voltage of 10 kV and layer length of 5 mm, E_b is set as

2 kV/mm. According to Ref. [38, 39], E_b of the non-linear FDC material can be adjusted by the percolation level [38], the shape and size of fillers [39]. Table 3 lists the electric field strength at P1–P4 under 10 kV DC voltage. By using a non-linear FDC layer, the electric field values with a non-linear FDC layer at all of the measurement points have been reduced similar to the effects that were obtained in a hypothetical high conductivity silicone gel. That is because the non-linear FDC material modified the conductivity of the silicone gel in the high electric field region, and increased the conductive current of this region, thus reducing the local electric field strength.

Table 3 also showed the electric field under the linear conductivity layer. Assuming that the conductivity of the covering layer could be increased to 3.5×10^{-9} S/m, the electric field will also be decreased to the same level as non-linear FDC layer. However, it is not sure how to get such high conductivity homogeneous silicone gel or another

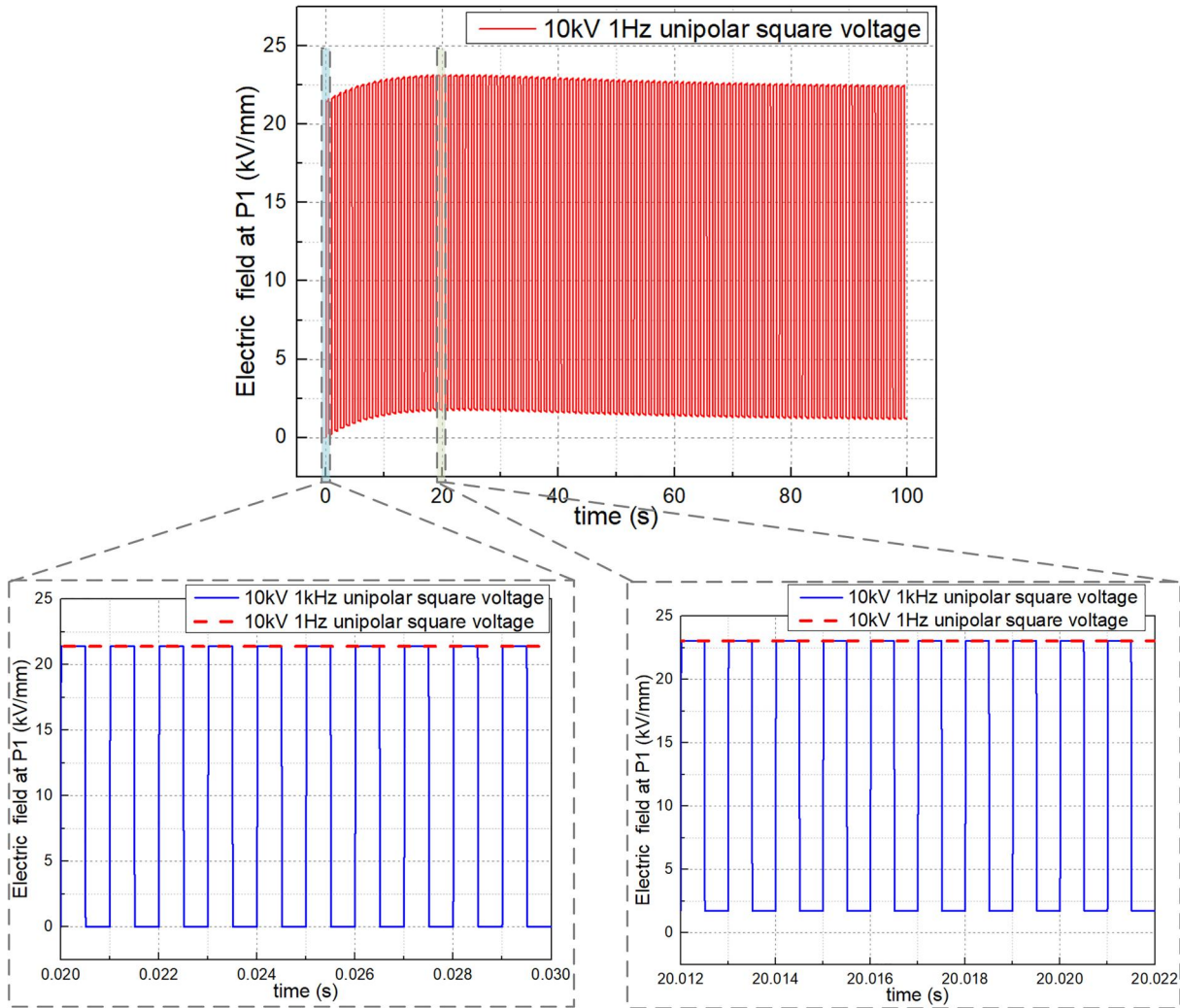


FIGURE 11 Comparison of electric fields at P1 under 1 Hz 10 kV unipolar square wave voltage and 1 kHz 10 kV unipolar square wave voltage

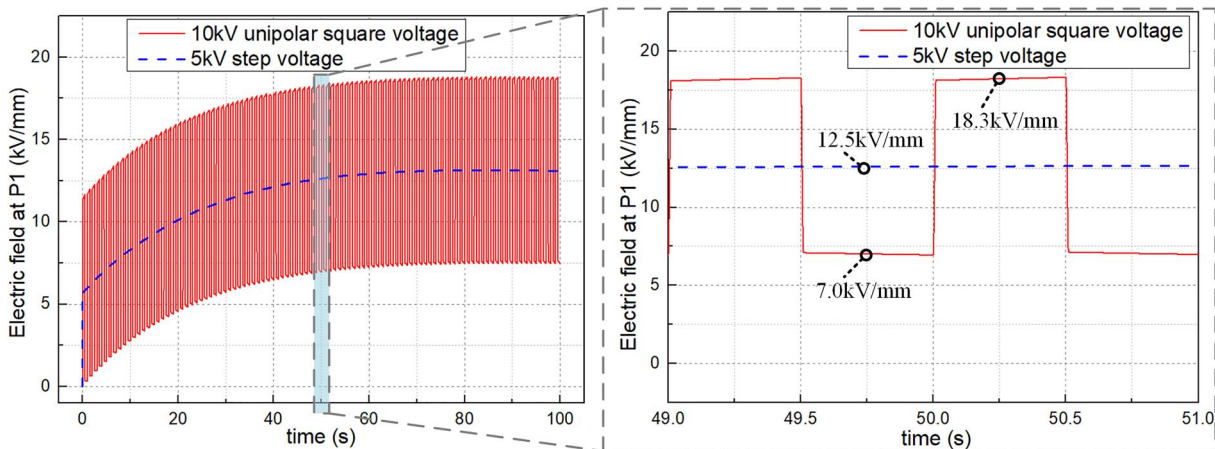


FIGURE 12 Electric fields at P1 under 1 Hz 10 kV unipolar square wave voltage and 5 kV step voltage when the gel relative permittivity is changed to 17.4

encapsulation which is suitable for power module packaging. Thus, we recommend mixing non-linear FDC fillers into silicone gel to obtain high FDC characteristics, such as ZnO

microvaristors, since the FDC characteristic of the composite with ZnO microvaristors fillers has been demonstrated in many research papers [27, 28, 40, 41].

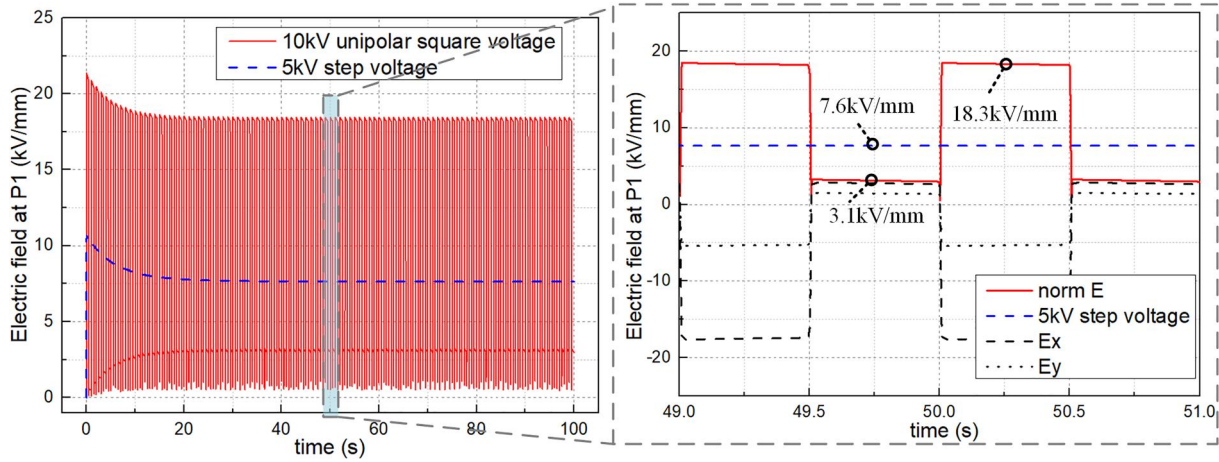


FIGURE 13 Electric fields at P1 under 1 Hz 10 kV unipolar square wave voltage and 5 kV step voltage when the gel conductivity is changed to 10^{-11} S/m

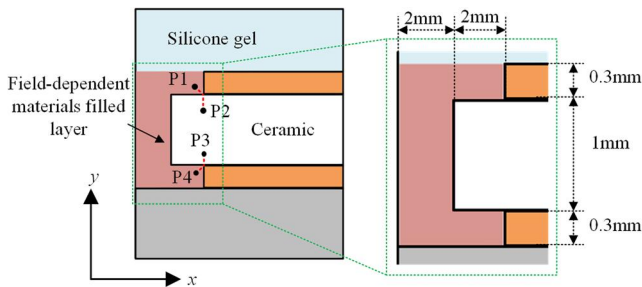


FIGURE 14 Schematic diagram of the simulation model for field-dependent material covering the edge of direct bonded copper

Next, we investigate the impact of non-linear permittivity fillers. The silicone gel filled with 15% barium titanate has been demonstrated to have good FDP properties [35], the relation between its relative permittivity ϵ_r , and $E(x, y)$ within the FDP layer is given by [35].

$$\epsilon_r = 6.4 + 1.3 * E(x, y) \quad (13)$$

The simulation uses Equation (13) as the relative permittivity of the modified silicone gel. Table 4 shows the maximum electric field value at P1-P4 under pure AC voltage. As we can see, the electric fields at P1 and P4 have been reduced by more than 50%, and the electric field at P2 and P3 also decreased by about 16%. The reason is that the relative permittivity of the high electric field region has been increased due to the FDP properties and affects the refraction of the field lines. Compared with the simulation results in Figure 8, the effect of FDP layer is smaller than that of linear high-permittivity materials. However, considering that the silicone gel host permittivity is fairly small, a large fill fraction or the use of particles with high permittivity will be needed. Since the FDP filler also may possess a high linear permittivity value, FDP materials are still a good choice to solve the electric field concentration under AC voltage.

TABLE 3 Electric field value at P1-P4 under 10 kV DC voltage

Case	Electric field value [kV/mm]			
	P1	P2	P3	P4
Without non-linear FDC layer	23.26	18.27	17.29	21.16
With non-linear FDC layer	2.97	11.61	10.16	1.99
With linear conductivity layer	3.06	11.86	9.35	0.03

Abbreviation: FDC, field-dependent conductivity.

TABLE 4 Electric field value at P1-P4 under 10 kV pure AC voltage

Case	Electric field value [kV/mm]			
	P1	P2	P3	P4
Without FDP layer	21.38	18.78	12.4	11.95
With FDP layer	11.11	15.26	10.37	5.57

Abbreviation: FDP, field-dependent permittivity.

4.2 | Single DBC substrate modules

For a single DBC substrate power module, the voltage stress between DC + terminal and baseplate is the DC-link voltage. If the electric field strength around DC + terminal is higher than the limitation of the insulation materials, the non-linear FDC layer should be implemented to decrease the electric field under DC voltage. For DC- terminal, there is no voltage stress, thus no mitigation measures are needed.

The voltage stress between the output terminal and ground is unipolar square wave voltage; as we discussed before, the maximum electric field value is not only determined by the average electric field value but also the peak-to-peak electric field value. Thus, both the conductivity and relative permittivity of the covering layer need to be increased. As reported in Ref. [27, 40], the relative permittivity of the silicone matrix filled with 40 volume percent ZnO microvaristor particles could be 12. That means compared with the initial gel, using the non-linear FDC layer could not only increase conductivity

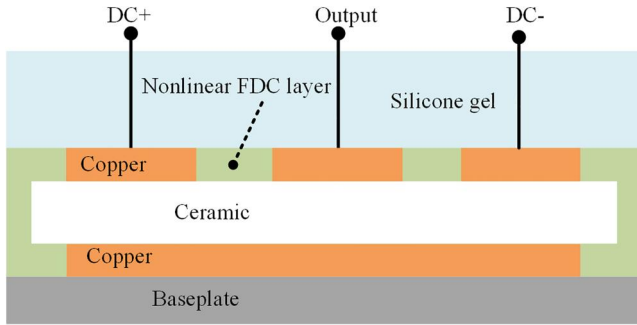


FIGURE 15 Illustration of coating non-linear field-dependent layer into power module with single direct bonded copper substrate

but also relative permittivity. Thus, the non-linear FDC layer can also efficiently relieve the electric field concentration around the output terminal. Considering the feasibility of fabrication, it is recommended to cover the entire DBC with the non-linear FDC layer. In this way, all the triple points can be covered, and it can save a certain cost since not a lot of non-linear FDC materials are needed. Finally, as illustrated in Figure 15, only a non-linear FDC layer is used in the single DBC substrate power module.

4.3 | Stacked DBC substrates modules

When using stacked DBC substrates in power module, there are new voltage configurations. We consider the local field strength concentration caused by the potential difference between adjacent conductors. Since the voltage of the middle copper layer has been fixed to half of the DC-link voltage, the voltage differences between up copper and middle copper have been reduced to half the value compared with the single DBC structure. Thus, there is no need to deal with the DC voltage stress between the DC+/DC- terminals and the middle copper layer, or DC voltage stress between the middle copper layer and the baseplate. For the output terminal, the voltage stress is bipolar square wave voltage. If the average value of the voltage is zero, there will be no electric field drift, it is the electrostatic field or capacitive field. As demonstrated before, increasing the relative permittivity of silicone gel could reduce the electric field. Thus, only FDP fillers need to be used around the output terminal to reduce the electric field. However, it is not easy to cover only the output terminal with the FDP layer. Thus, it is recommended to cover the entire DBC with the FDP layer as illustrated in Figure 16.

5 | CONCLUSION

Electric field control methods at the triple point in the middle voltage power module were reviewed; it was found that the stacked DBC substrates and coating field-dependent materials are effective ways to reduce the electric field strength and are easy to be implemented. By explaining the

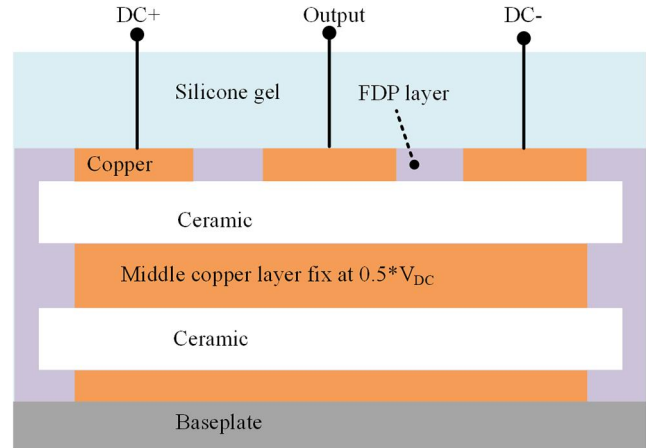


FIGURE 16 Illustration of coating non-linear field-dependent layer into power module with stacked direct bonded copper substrates

electric field drift phenomenon with the charge relaxation theory, the influence factors of the electric field under different voltage stresses have been studied by simulation. Under the bipolar square wave voltage, only the relative permittivity influences the electric field. Both relative permittivity and conductivity of materials can influence the electric field strength under unipolar square wave voltage. In order to reduce the high electric field at the triple point, it is recommended to cover the entire DBC with the non-linear FDC layer in the single DBC substrate power module, and in the stacked DBC substrates power module it is suggested to cover the DBC with the FDP layer. These recommendations can provide guidance to the power module designers on how to reduce the high electric field at the triple point under different module structures.

ACKNOWLEDGMENTS

This work was supported by the National Natural Science Foundation of China (52,077,094).

ORCID

Zhizhao Huang  <https://orcid.org/0000-0002-3805-2979>

REFERENCES

1. Singh, R., et al.: Large area, ultra-high voltage 4H-SiC p-i-n rectifiers. *IEEE Trans. Electron. Devices.* 49(12), 2308–2316 (2002)
2. Madhusoodhanan, S., et al.: Solid-state transformer and MV grid tie applications enabled by 15 kV SiC IGBTs and 10 kV SiC MOSFETs based multilevel converters. *IEEE Trans. Ind. Appl.* 51(4), 3343–3360 (2015)
3. Casady, J.B., et al.: New Generation 10 kV SiC power MOSFET and diodes for industrial applications. In: *PCIM Europe*, pp. 1–8. (2015)
4. Ghassemi, M.: High power density technologies for large generators and motors for marine applications with focus on electrical insulation challenges. *High Volt.* 5(1), 7–14 (2020)
5. Gao, Y., et al.: Study on lightning protection scheme of multi-terminal MMC-MVDC distribution system. *High Volt.* 5(5), 605–613 (2020)
6. Passmore, B., O'Neal, C.: High-voltage SiC power modules for 10–25 kV applications. *Power Electron. Europe Mag.* (1), 22–24 (2016)
7. Wang, G., Huang, A., Li, C.: ZVS range extension of 10 A 15 kV SiC MOSFET based 20 kW dual active half bridge (DHB) DC-DC converter.

- In: IEEE Energy Conversion Congress and Exposition, Raleigh, NC, pp. 1533–1539. (2012)
8. Bęczkowski, S., et al.: 10kV SiC MOSFET split output power module. In: 17th European Conference on Power Electronics and Applications (EPE'15 ECCE-Europe), Geneva, pp. 1–7 (2015)
 9. Sato, M., et al.: Degradation process of silicone-gel by internal surface discharges. In: IEEE 18th International Conference on Dielectric Liquids (ICDL), Bled, pp. 1–4 (2014)
 10. Emersic, C., et al.: Degradation of conformal coatings on printed circuit boards due to partial discharge. IEEE Trans. Dielectr. Electr. Insul. 23(4), 2232–2240 (2016)
 11. Sato, M., et al.: Surface discharges in silicone gel on AlN substrate. IEEE Trans. Dielectr. Electr. Insul. 23(1), 494–500 (2016)
 12. Bayer, C., et al.: Enhancing partial discharge inception voltage of DBCs by geometrical variations based on simulations of the electric field strength. In: International Conference on Integrated Power Electronics Systems, Nuremberg, Germany, pp. 1–5 (2016)
 13. Mitic, G., Lefranc, G.: Localization of electrical-insulation and partial-discharge failures of IGBT modules. IEEE Trans. Ind. Appl. 38(1), 175–180 (2002)
 14. Mitic, G., Licht, T., Lefranc, G.: IGBT module technology with high partial discharge resistance. IEEE Conf. Ind. Appl. 3, 1899–1904 (2001)
 15. Fabian, J.-H., Hartmann, S., Hamidi, A.: Analysis of insulation failure modes in high power IGBT modules. In: 14th IAS Annual Meeting, Conference Record of the 2005 Industry Applications Conference, Kowloon, Hong Kong, China, vol. 2, pp. 799–805 (2005)
 16. Bayer, C., et al.: Simulation of the electric field strength in the vicinity of metallisation edges on dielectric substrates. IEEE Trans. Dielectr. Electr. Insul. 22(1), 257–265 (2015)
 17. Hohlfeld, O., et al.: Stacked substrates for high voltage applications. In: 2012 7th International Conference on Integrated Power Electronics Systems, (CIPS), pp. 1–4. IEEE, Nuremberg (2012)
 18. Bayer, C.F., et al.: Stacking of insulating substrates and a field plate to increase the PDIV for high voltage power modules. In: IEEE 66th Electronic Components and Technology Conference (ECTC), Las Vegas, NV, pp. 1172–1178 (2016)
 19. DiMarino, C.: Design and validation of a high-density 10 kV silicon carbide MOSFET power module with reduced electric field strength and integrated common-mode screen, Ph.D. dissertation. Virginia Polytechnic Institute and State University (2019)
 20. Deshpande, A., et al.: Stacked DBC cavitied substrate for a 15-kV half-bridge power module. In: IEEE International Workshop on Integrated Power Packaging, Toulouse, France, pp. 12–17 (2019)
 21. Reynes, H., Buttay, C., Morel, H.: Protruding ceramic substrates for high voltage packaging of wide bandgap semiconductors. In: IEEE 5th Workshop on Wide Bandgap Power Devices and Applications (WiPDA), Albuquerque, NM, pp. 404–410 (2017)
 22. Hourdequin, H., et al.: Design of packaging structures for high voltage power electronics devices: electric field stress on insulation. In: IEEE International Conference on Dielectrics (ICD), Montpellier, pp. 999–1002 (2016)
 23. Valdez-Nava, Z., et al.: Ceramic substrates for high voltage power electronics: past, present and future. In: IEEE International Workshop on Integrated Power Packaging (IWIPP), Toulouse, France, pp. 91–96 (2019)
 24. Frey, D., et al.: Electric field investigation in high voltage power modules using finite element simulations and partial discharge measurements. In: Industry Applications Society Annual Meeting, pp. 1000–1005 (2003)
 25. Ghassemi, M.: Electrical insulation weaknesses in wide bandgap devices. In: Albarracin, R. (ed.), Simulation and Modelling of Electrical Insulation Weaknesses in Electrical Equipment, London, UK, pp. 129–149. (2018)
 26. Christen, T., Donzel, L., Greuter, F.: Nonlinear resistive electric field grading part 1: theory and simulation. IEEE Electr. Insul. Mag. 26(6), 47–59 (2010)
 27. Donzel, L., Greuter, F., Christen, T.: Nonlinear resistive electric field grading. Part 2: Materials and applications. IEEE Electr. Insul. Mag. 27(2), 18–29 (2011)
 28. Donzel, L., Schuderer, J.: Nonlinear resistive electric field control for power electronic modules. IEEE Trans. Dielectr. Electr. 19(3), 955–959 (2012)
 29. Tousi, M.M., Ghassemi, M.: Electric field control by nonlinear field dependent conductivity dielectrics characterisation for high voltage power module packaging. In: IEEE International Workshop on Integrated Power Packaging, Toulouse, France, pp. 54–58 (2019)
 30. Tousi, M.M., Ghassemi, M.: Nonlinear field dependent conductivity materials for electric field control within next-generation wide bandgap power electronics modules. In: IEEE Electrical Insulation Conference (EIC), Calgary, AB, Canada, pp. 63–66 (2019)
 31. Tousi, M.M., Ghassemi, M.: Nonlinear resistive electric field grading in high-voltage, high-power wide bandgap power module packaging. In: IEEE Energy Conversion Congress and Exposition (ECCE), Baltimore, MD, USA, pp. 7124–7129 (2019)
 32. Tousi, M.M., Ghassemi, M.: Characterisation of nonlinear field-dependent conductivity layer Coupled with protruding substrate to address high electric field issue within high-voltage high-density wide bandgap power modules. IEEE J. Emerg. Sel. Topics Power Electron. 8(1), 343–350 (2020)
 33. Waltrich, U., et al.: Enhancement of the partial discharge inception voltage of ceramic substrates for power modules by trench coating. In: International Conference on Electronics Packaging (ICEP), Sapporo, pp. 536–541 (2016)
 34. Ghassemi, M.: Electrical insulation weaknesses in wide bandgap devices. In: Sánchez, R. A. (ed.), Simulation and Modelling of Electrical Insulation Weaknesses in Electrical Equipment, Chapter 6, pp. 129–149. IntechOpen, UK (2018)
 35. Wang, N., et al.: Partial discharge control in a power electronic module using high permittivity non-linear dielectrics. IEEE Trans. Dielectr. Electr. Insul. 17(4), 1319–1326 (2010)
 36. Diahm, S., et al.: An original in-situ way to build field grading materials (FGM) with permittivity gradient using electrophoresis. In: IEEE 2nd International Conference on Dielectrics (ICD), Budapest, Hungary, pp. 1–4 (2018)
 37. Mukherjee, S., et al.: Towards partial discharge reduction by corner correction in power module layouts. In: 2018 IEEE 19th Workshop on Control and Modeling for Power Electronics (COMPEL), Padua, pp. 1–8 (2018)
 38. Yang, X., et al.: Understanding the percolation characteristics of nonlinear composite dielectrics. Sci. Rep. 6, 30597 (2016)
 39. Yang, X., et al.: Grading electric field in high voltage insulation using composite materials. IEEE Electr. Insul. Mag. 34(1), 15–25 (2018)
 40. Donzel, L., et al.: Silicone composite for HV applications based on microvaristors. In: IEEE International Conference on Solid Dielectrics, pp. 403–406. IEEE, Toulouse. (2004)
 41. Yang, X., Hu, J., He, J.L.: Adjusting nonlinear characteristics of ZnO-silicone rubber composites by controlling filler's shape and size. In: IEEE International Conference on Dielectrics (ICD), Montpellier, pp. 313–317 (2016)

How to cite this article: Huang, Z., et al.: Mitigation measures of the electric field in the medium-voltage power module: effect of voltage types and recommendations for designers. High Volt. 6(5), 836–849 (2021). <https://doi.org/10.1049/hve2.12104>